# Impact of Doppler effects on the distribution of ICRH accelerated ions

(article starts on next page)

PURPOSE-LED
PUBLISHING™

**PAPER • OPEN ACCESS**

# Impact of Doppler effects on the distribution of ICRH accelerated ions

To cite this article: Lukas Bähner *et al* 2025 *Plasma Phys. Control. Fusion* **67** 045024

View the article online for updates and enhancements.

## You may also like

# Impact of Doppler effects on the distribution of ICRH accelerated ions

## Lukas Bähner[1],*, Thomas Johnson[1], Lars-Göran Eriksson[2] and Björn Zaar[1]

[1] Department of Electrical Engineering, KTH Royal Institute of Technology, Stockholm SE-11428, Sweden
[2] Department of Space, Earth and Environment, Chalmers University of Technology, Gothenburg, SE-41296, Sweden

E-mail: bahner@kth.se

CrossMark

## Abstract
Ion cyclotron resonance heating (ICRH) has the potential of providing efficient ion heating of reactor grade fusion plasmas especially during the start-up phase. In order to assess such heating scenarios, ICRH modelling is required. However, the physics is complex and certain elements are not universally taken into account in ICRH modelling. In this paper we discuss the importance of including Doppler shift displacements of resonance points away from the cold resonance (i.e. where $\omega = n\Omega_c$) in Fokker–Planck calculations of the distribution function of resonating ions. In particular, the resonant interaction time and the wave electric field varies with the local Doppler shifted resonance positions. The importance of accounting for these variations in Fokker–Planck modelling is investigated. Furthermore, it is shown how these effects can be included in a simplified Fokker–Planck treatment that is sufficiently quick for integrated modelling frameworks of fusion plasmas. Because 2D effects in velocity space play a crucial role in determining Doppler shifts, we employ a model of the anisotropy of the non-thermal distribution function. Simulation results show that taking the Doppler effects into account in Fokker–Planck modelling can have a significant impact on the distribution functions of fast ions and important quantities, such as the collisional power transfer to the background plasma. This is especially important in cases where the poloidal variation of the left-hand component of the wave electric field is strong.

Keywords: ICRH, Fokker–Planck, Pitch angle average, Doppler effect, quasi-linear

## 1. Introduction

Auxiliary heating of tokamak fusion plasmas by *y* ion cyclotron resonance heating (ICRH) has a proven track record and its potential for providing effective ion heating has been demonstrated in DT plasmas by [1–3]. In fact, out of the current auxiliary heating methods for tokamaks, it is the only one

that could provide significant ion heating during the start-up phase of a reactor grade plasma. There are also other aspects of ITER that could be of interest for ITER and a demonstration (DEMO) reactor, such as current drive, profile and impurity control and wall conditioning [4–7]. It is therefore of interest to continue to explore the potential of ICRH, not least by simulating its impact on fusion plasmas. To this end, not only models with a high degree of physics fidelity [8–12] should be developed, but also simplified models which are suitable for inclusion in frameworks for integrated modelling of fusion plasmas, such as PION [13] and FoPla [14]. It is especially important when developing simplified modelling to assess key physics effects that should be included in the modelling. In this paper, the effect of the Doppler shifted wave frequency on the distribution function of the resonating ions is

investigated. For simplicity, the analysis presented here is limited to the thin banana width limit, which may be appropriate for a large reactor-grade plasma away from the most central region. However, finite orbit width effects may play a significant role in smaller devices requiring at least the solution of a three-dimensional orbit averaged Fokker–Planck equation including a collision operator and a quasi-linear operator, see e.g. [15]. While such modelling has proved indispensable in studying many detailed aspects of ICRH heating, for example by [16–20], it is not necessary for assessing the salient features of the Doppler effect on the distribution function of resonating ions.

An individual ion following its guiding centre orbit in a tokamak receives a 'kick' in energy in the vicinity of a resonance point, where the phase $\nu$ of the cyclotron motion relative to the Doppler shifted wave oscillation is stationary, i.e. $\ddot{\nu} = n\Omega_c(\mathbf{r}_{res}) + k_\parallel v_\parallel - \omega = 0$. Here $\omega$ is the angular wave frequency, $\Omega_c$ the cyclotron frequency, $\mathbf{r}_{res}$ the spatial location of the resonance, $n$ the harmonic number of the resonance, while $k_\parallel$ and $v_\parallel$ are the wave vector and velocity components parallel to the magnetic field. As a result of including the Doppler shift, $k_\parallel v_\parallel$, the resonance is shifted away from the cold resonance, $\omega = n\Omega_c$. There are two major effects associated with this that need to be accounted for: (i) the effective time of a resonant interaction (in terms of a stationary phase approximation) depends inversely on $\sqrt{\ddot{\nu}}$ and varies strongly with the spatial location of the resonance point; (ii) in certain scenarios the wave polarisation is more advantageous away from the cold resonance and also the magnitude of the wave electric field may vary significantly spatially. Thus, a full 2D Fokker–Planck code that uses only the flux surface averaged absorbed power density and a ratio $E_-/E_+$ at the cold resonance as input does not capture the correct physics. Here $E_-$ and $E_+$ are the right and left hand polarised components of the wave electric field respectively. In the current paper we develop a Fokker–Planck model for the resonating ions that incorporates the Doppler effect. Furthermore, in order to make the scheme suitable for integrated modelling, the 2D character of the distribution function needed for the analysis is described by the pitch angle distribution proposed by Dendy *et al* [21] together with a solution of an appropriately pitch-angle averaged Fokker–Planck equation. The latter takes into account the anisotropy provided by the model for the pitch angle distribution. For numerical evaluation of the quasilinear diffusion coefficient in the Fokker–Planck equation, wave fields have been taken from the full wave code FEMIC [22].

We find that the impact of the Doppler effect on important quantities for integrated modelling, such as the collisional power transfer to the background ions and electrons, can be significant when an ion–ion hybrid layer (IIHL) is formed by the presence of at least two ion species.

## 2. Fokker–Planck theory

### 2.1. Bounce averaged Fokker–Planck equation

The evolution of the orbit averaged distribution function, $f_0$, of ions resonating with ICRH waves in a toroidal plasma can be described by a three-dimensional orbit averaged Fokker–Planck equation,

$$\frac{\partial f_0}{\partial t} = \langle C(f_0) \rangle + \langle Q(f_0) \rangle \tag{1}$$

as presented by [15]. Here, $\langle C(f_0) \rangle$ is the collision operator and $\langle Q(f_0) \rangle$ is the quasi-linear operator representing the effect of the wave-particle interaction on the distribution function. The distribution function, $f_0$, is a function of three invariants of the unperturbed particle motion, e.g. the velocity, $v$, the normalised magnetic moment, $\Lambda = \mu B_0/W = (1 - \xi^2)B_0/B$ and the canonical toroidal angular momentum $P_\phi = mRv_\parallel B_\phi/B + Ze\psi$. In these definitions, $\mu = m(v^2 - v_\parallel^2)/(2B)$ is the magnetic moment, $B_\phi$ is the toroidal component of the magnetic field and $B_0$ is the magnetic field strength at a reference point. The particle energy is denoted by $W = mv^2/2$, and $\xi = v_\parallel/v$ is the pitch. Note that $R$ is the major radius coordinate in the toroidal geometry and $\psi$ is the poloidal flux. The quasi-linear description of the wave-particle interaction is valid provided the relative phase between the waves and the Larmor motion of the resonating ions is sufficiently randomised between successive transits of an orbit as discussed in [23–25], and we assume that this is the case throughout this paper.

Resolving the full three-dimensional orbit averaged Fokker–Planck equation is cumbersome and numerically costly. It is therefore not suitable for the rapid calculations needed for instance in integrated modelling. For this reason, we seek to simplify the equation and aim at a reduced model where only a one-dimensional differential equation needs to be solved. The first step in the simplification procedure is to neglect spatial transport of the resonating ions (either by neoclassical effects or by wave-induced transport). Furthermore, we adopt the small banana width limit. Wide orbit effects are important when fast ions on wide orbits can transfer their power by collisions predominantly in the colder, outer regions of the plasma. Such effects are important especially in smaller fusion devices, but are less important in bigger devices such as JET or ITER. With the assumption of small banana orbits, the distribution function on a given flux surface is a function of the velocity and the normalised magnetic moment, $f_0 = f_0(v, \Lambda)$. Then, the operator, $\langle Q(f_0) \rangle$, reduces to [15]

$$\langle Q(f_0) \rangle = \frac{1}{\sqrt{g}} \frac{\partial}{\partial v}\left[ \sqrt{g}D^{vv}\frac{\partial f_0}{\partial v} \right] + \frac{1}{\sqrt{g}}\frac{\partial}{\partial v}\left[ \sqrt{g}D^{v\Lambda}\frac{\partial f_0}{\partial \Lambda} \right]$$
$$+ \frac{1}{\sqrt{g}}\frac{\partial}{\partial \Lambda}\left[ \sqrt{g}D^{\Lambda v}\frac{\partial f_0}{\partial v} \right] + \frac{1}{\sqrt{g}}\frac{\partial}{\partial \Lambda}\left[ \sqrt{g}D^{\Lambda\Lambda}\frac{\partial f_0}{\partial \Lambda} \right], \tag{2}$$

where $\sqrt{g} = v^3 \tau_B/(4\pi Ze B_0)$ is the Jacobian arising by changing from action variables to the invariants of motion $(v, \Lambda, P_\phi)$, and $\tau_B$ is the bounce time. The diffusion coefficients are

$$D^{vv} = \left( \frac{\omega}{mv} \right)^2 D_0,$$

$$D^{v\Lambda} = D^{\Lambda v} = 2 \frac{\omega \left( n\Omega_{c,0} - \Lambda\omega \right)}{m^2 v^3} D_0, \quad (3)$$

$$D^{\Lambda\Lambda} = \left( 2 \frac{n\Omega_{c,0} - \Lambda\omega}{mv^2} \right)^2 D_0,$$

where $\Omega_{c,0}$ is the cyclotron frequency evaluated at the reference magnetic field, $B_0$. In the diffusion coefficients, there is

$$D_0 = \frac{1}{2\tau_B} \left( \frac{Ze}{\omega} \right)^2 \sum_n \left| \oint_{\text{orbit}} v_\perp E_e e^{i\nu} dt \right|^2, \quad (4)$$

where the effective electric field strength is defined as $E_e = E_+ J_{n-1} + E_- J_{n+1}$. $J_n$ is the $n$th order Bessel function of the first kind with the argument $k_\perp \rho_L = k_\perp v_\perp / \Omega_c$ evaluated at the stationary points, where $k_\perp$ and $v_\perp$ are the wave vector and the velocity component perpendicular to the magnetic field. If we use the stationary phase method as done in [23, 24, 26], only stationary points of the phase contribute to the orbit integral. Consequently, we may write

$$D_0 = \frac{1}{2\tau_B} \left( \frac{Ze}{\omega} \right)^2 \sum_{n,s} \left| v_\perp E_e \sqrt{\frac{2\pi}{|\ddot{\nu}|}} \right|^2, \quad (5)$$

where we sum over all stationary points $s$ and the phase $\nu$ has been approximated using a Taylor expansion to obtain the resonant interaction time $\sqrt{2\pi / |\ddot{\nu}|}$.

### 2.2. Pitch angle averaged Fokker–Planck equation

Here, the pitch angle average of a quantity $X$ is defined with an integral operator $I$,

$$\langle X \rangle_\Lambda = I(X) / I(1), \quad I(X) = \int X d^3 r d^3 v, \quad (6)$$

where the integration is performed over a narrow range of flux surfaces, $(\psi, \psi + d\psi)$, and velocities, $(v, v + dv)$. For functions of the invariants of motion, $X(v, \Lambda, P_\phi)$, it is useful to change the integration variables to the invariants $(v, \Lambda, P_\phi)$ and the canonical angles. In the small banana width limit, $P_\phi = Ze\psi$. This enables a transformation from $(v, \Lambda, P_\phi)$ to $(v, \Lambda, V)$, where $V(\psi)$ is the volume enclosed by a flux surface $\psi$. Integrating over the canonical angles, the phase space volume element can be replaced by

$$d^3 r d^3 v \rightarrow \left( 4\pi v^2 dv \right) \left( a\sqrt{g} d\Lambda \right) dV. \quad (7)$$

This formulation introduces an additional factor $a = 2\pi^2 Ze / (v^2 V')$ to the Jacobian, where $V' = dV/d\psi$. Then, $I(X)$ can be written as

$$I(X) = \left( 4\pi v^2 dv \right) dV \sum_\sigma \int_0^{\Lambda_{\max}} X a\sqrt{g} d\Lambda, \quad (8)$$

where $\Lambda_{\max} = B_0 / B_{\min}$ is the maximum value of $\Lambda$ and $\sum_\sigma$ takes care of the two possible signs $\sigma = \pm 1$ of the pitch associated with each $\Lambda$. Now the average can be written as

$$\langle X \rangle_\Lambda = \frac{1}{\ell} \sum_\sigma \int_0^{\Lambda_{\max}} X v\tau_B d\Lambda, \quad (9)$$

where $v\tau_B$ is velocity independent in the small banana width limit and the normalization length $\ell$ is given by

$$\ell = \sum_\sigma \int_0^{\Lambda_{\max}} v\tau_B d\Lambda. \quad (10)$$

In this work, the distribution function on a given flux surface is separated into a velocity distribution, $\eta(v)$, and a pitch angle distribution, $\chi(v, \Lambda)$, where the latter is normalised such that $\langle \chi(v, \Lambda) \rangle_\Lambda = 1$. The distribution can then be written as

$$f_0(v, \Lambda) = \eta(v) \chi(v, \Lambda). \quad (11)$$

In section 2.4, an analytical model for $\chi(v, \Lambda)$ is introduced, thus the task here is to find an equation for $\eta(v)$.

The pitch angle average of the collision operator eliminates the pitch angle scattering term, leaving

$$\langle\langle C(f_0) \rangle\rangle_\Lambda = \frac{1}{v^2} \frac{\partial}{\partial v} v^2 \left( \kappa\eta + \frac{\beta}{2} \frac{\partial\eta}{\partial v} \right). \quad (12)$$

Here $\kappa = -\alpha + \frac{1}{2v^2} \frac{d}{dv} \left( \beta v^2 \right)$, where $\alpha$ and $\beta$ are given e.g. by [27] and are functions of the velocity $v$. The pitch angle averaged quasi-linear operator takes the form

$$\langle\langle Q(f_0) \rangle\rangle_\Lambda = \frac{1}{v^2} \frac{\partial}{\partial v} v^2 \left( d\eta + D \frac{\partial\eta}{\partial v} \right). \quad (13)$$

where the RF diffusion coefficient is

$$D := \langle D^{vv} \chi \rangle_\Lambda = \left\langle \sum_{n,s} \frac{1}{2\tau_B} \left| \frac{ZeE_e}{m} \frac{v_\perp}{v} \sqrt{\frac{2\pi}{|\ddot{\nu}|}} \right|^2 \chi(v, \Lambda) \right\rangle_\Lambda, \quad (14)$$

and the RF drift coefficient is

$$d := \left\langle D^{vv} \frac{\partial\chi}{\partial v} + D^{v\Lambda} \frac{\partial\chi}{\partial\Lambda} \right\rangle_\Lambda$$

$$= \left\langle \sum_{n,s} \frac{1}{2\tau_B} \left| \frac{ZeE_e}{m} \frac{v_\perp}{v} \sqrt{\frac{2\pi}{|\ddot{\nu}|}} \right|^2 \left( \frac{\partial\chi}{\partial v} + \frac{2\left(\Lambda_{\text{res}} - \Lambda\right)}{v} \frac{\partial\chi}{\partial\Lambda} \right) \right\rangle_\Lambda, \quad (15)$$

with $\Lambda_{\text{res}} = B_0 / B_{\text{res}}$ and the magnetic field strength at the cold resonance $(\omega = n\Omega_c)$, $B_{\text{res}}$. In summary, diffusion in $v$ and $\Lambda$ appears due to the $\Lambda$-average as a drift in $v$ when an anisotropic pitch angle distribution $\chi$ is present. The quasi-linear coefficients above depend on the velocity $v$ and on the flux surface label for each ion species.

## 2.3. Resonant poloidal angle average

A problem that arises when evaluating (14) and (15) are the singularities when $\ddot{\nu} = 0$. These singularities are not present in equation (4), but are introduced by the stationary phase method. There are orbits that have their point of stationary phase ($\dot{\nu} = 0$) where also the phase acceleration vanishes ($\ddot{\nu} = 0$). At such *tangential* resonances, the phase remains stationary, and ions keep being accelerated, causing the expression for the diffusion coefficient to diverge. Higher order expansions in the stationary phase method resolve singularities at tangential resonances [26, 28]. This method introduces Airy functions that are needed to evaluate the resonant interaction time. However, in pitch angle averaged coefficients these singularities become apparent. Thus, higher order expansions are not needed to resolve them. We now show that a change of coordinate from the constant of motion $\Lambda$ to a more suitable one resolves singularities of the resonant interaction time.

A useful variable for that purpose is the *resonant poloidal angle*, $\theta_{\text{res}}$, defined as the equal arc-length poloidal angle, for which the resonance condition $\dot{\nu} = 0$ is fulfilled. The relation between $\theta_{\text{res}}$ and $\Lambda$ can be found by considering the parallel velocity required to Doppler shift the cyclotron resonance along a flux surface to a poloidal angle $\theta_{\text{res}}$, i.e.

$$v_{\parallel}(\theta_{\text{res}}) = \frac{\omega - n\Omega_{\text{c}}(\theta_{\text{res}})}{k_{\parallel}(\theta_{\text{res}})}. \tag{16}$$

Consequently, the value of $\Lambda$ corresponding to resonance at $\theta_{\text{res}}$ can be expressed as

$$\Lambda(\theta_{\text{res}}) = \left(1 - \frac{v_{\parallel}^2(\theta_{\text{res}})}{v^2}\right)\frac{B_0}{B(\theta_{\text{res}})}. \tag{17}$$

The value of $\sigma$ corresponding to resonance at $\theta_{\text{res}}$ is given by the sign of $v_{\parallel}$ in equation (16). For each velocity $v$, harmonic number $n$ and wave mode, $\Lambda$ and $\sigma$ are functions of $\theta_{\text{res}}$. This mapping is illustrated in figure 1, where the functions are numerically evaluated for a JET-like plasma at different energies $W$ on a selected flux surface $\psi$. Note that at low energies, valid regions of $\theta_{\text{res}}$ do not cover the whole flux surface, and that in general not all combinations of $\Lambda$ and $\sigma$ are resonant, e.g. at high energies, most passing orbits are not resonant. In order to find how $d\Lambda/d\theta_{\text{res}}$ is related to $\ddot{\nu}$ it is useful to start with the resonance function, $f_{\text{res}}(\theta, \Lambda) := \dot{\nu} = n\Omega_{\text{c}} + k_{\parallel}v_{\parallel} - \omega$, on a given flux surface and for a given velocity. The differential of this function is given by

$$df_{\text{res}} = f_{\theta}d\theta + f_{\Lambda}d\Lambda, \tag{18}$$

where the derivatives $f_{\theta}$ and $f_{\Lambda}$ are calculated in appendix A. Equation (18) can be used to describe how the resonance is displaced when $\Lambda$ is perturbed. In this scenario we are tracing the resonance, thus $f_{\text{res}} = 0$, $df_{\text{res}} = 0$ and $\theta = \theta_{\text{res}}$. Consequently,

$$d\Lambda = \frac{f_{\theta_{\text{res}}}}{-f_{\Lambda}}d\theta_{\text{res}} = \frac{B_0}{B_{\theta}}\frac{L\ddot{\nu}}{\pi k_{\parallel}v^2}d\theta_{\text{res}} \tag{19}$$

where $L$ is the length of the flux surface in the poloidal cross section and the poloidal component of the magnetic field is denoted by $B_{\theta}$. It is possible to use this change of coordinates for averaging of functions that are evaluated at resonances, i.e. the quasi-linear drift and diffusion coefficients in (14) and (15). Considering the integration over domains with positive and negative sign $\sigma$ of the pitch in (9), the factor $1/|\ddot{\nu}|$ is cancelled by the factor $\ddot{\nu}$ in (19). The pitch angle averaged RF diffusion coefficient can then be written as an integral over $\theta_{\text{res}}$

$$D = \sum_n \int_{\Delta_{\text{res}}} \left|\frac{L}{\ell}\frac{B}{B_{\theta}}\frac{\Lambda}{k_{\parallel}v}\right|\left|\frac{ZeE_{\text{e}}}{m}\right|^2 \chi \, d\theta_{\text{res}}, \tag{20}$$

and the pitch angle averaged RF drift coefficient becomes

$$d = \sum_n \int_{\Delta_{\text{res}}} \left|\frac{L}{\ell}\frac{B}{B_{\theta}}\frac{\Lambda}{k_{\parallel}v}\right|\left|\frac{ZeE_{\text{e}}}{m}\right|^2$$
$$\times \left(\frac{\partial\chi}{\partial v} + \frac{2(\Lambda_{\text{res}} - \Lambda)}{v}\frac{\partial\chi}{\partial\Lambda}\right) d\theta_{\text{res}}. \tag{21}$$

where $\Delta_{\text{res}}$ represents the resonant regions the flux surface, see e.g. figure 1. To ensure that the power transfer from the wave to the resonant ions is consistently described in the Fokker–Planck model and the wave solver, the quasi-linear coefficients $d$ and $D$ may be normalised. The details of this normalisation are described in section 3.

## 2.4. Solution to the Fokker–Planck equation and model for the anisotropy

The pitch angle averaged Fokker–Planck equation is one-dimensional in velocity $v$ on each flux surface $\psi$. In steady-state, we can solve for the distribution function for each $\psi$ by direct integration, as shown in [27, 29]

$$\eta(v) = \eta(0)\exp\left(-\int_0^v \frac{\kappa + d}{\beta/2 + D}dv'\right), \tag{22}$$

where $\eta(0)$ is a normalisation to match the ion density $n_i$.

In order to perform the averages in (20) and (21), we need a model for the pitch angle distribution $\chi(v, \Lambda)$. To avoid solving the two-dimensional Fokker–Planck equation, we propose an ad-hoc model for the pitch angle distribution, which is similar to the bi-Maxwellian distribution proposed in [21] and given by

$$\chi(v, \Lambda) = \chi_0(v)\left(\frac{m}{2\pi}\right)^{3/2}\frac{1}{T_{\perp}T_{\parallel}^{1/2}}$$
$$\times \exp\left(-\frac{W_{\perp}}{T_{\perp}} - \frac{|W_{\parallel}|}{T_{\parallel}} - \frac{W_{\parallel} - |W_{\parallel}|}{T_{\perp}}\right), \tag{23}$$

where $W_{\perp} = \mu B_{\text{res}}$, $W_{\parallel} = W - W_{\perp}$, $B_{\text{res}} = m\omega/(nZe)$. $T_{\parallel}$ and $T_{\perp}$ denote temperatures (in units of energy) parallel and perpendicular to the magnetic field, respectively, at $B = B_{\text{res}}$. The factor $\chi_0(v)$ is defined such that $\langle\chi\rangle_{\Lambda} = 1$. Note that although $W_{\perp}$ and $W_{\parallel}$ have units of energy, they are the same as the perpendicular and parallel energies only at the resonance,
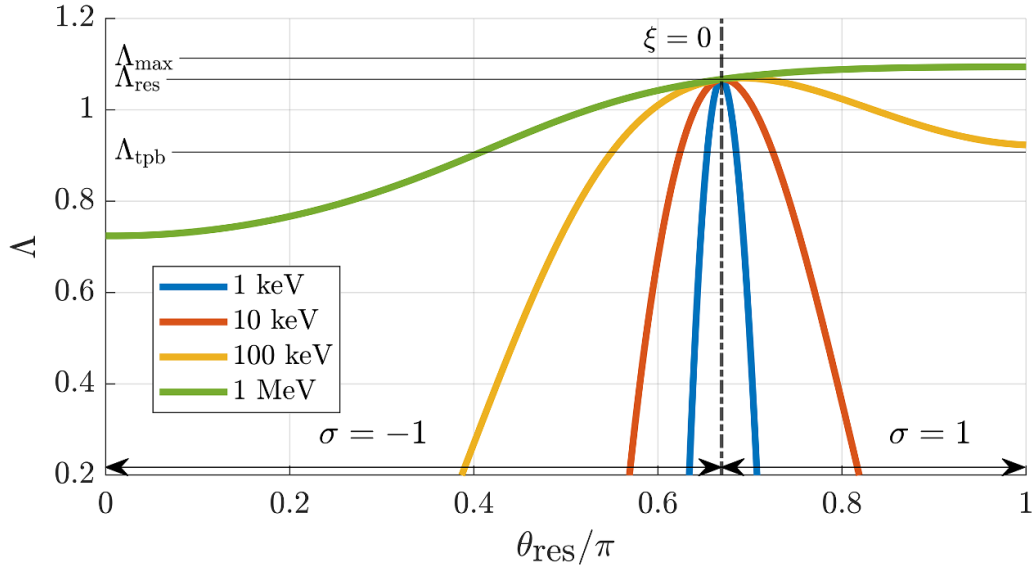
**Figure 1.** Example for constant of motion $\Lambda$ as function of resonant poloidal angle $\theta_{res}$ in $[0, \pi]$, where the cold resonance $\omega = n\Omega_c$ is marked with $\xi = 0$. The angle $\theta_{res} = 0$ is in the equatorial plane on the *high* field side and increases anti-clockwise. The regions with positive $\sigma = 1$ and negative $\sigma = -1$ pitch are marked with black arrows. For reference, the maximum value $\Lambda_{max}$, the value at the cold resonance $\Lambda_{res}$ and the trapped-passing boundary $\Lambda_{tpb}$ are marked.

$B = B_{res}$. In fact, when $\Lambda > \Lambda_{res}$ then $W_{\parallel} < 0$. The distribution function (23) differs from the one proposed by [21] by the third term in the exponent, which ensures that the distribution function is isotropic when $T_{\perp} = T_{\parallel}$. This affects only deeply trapped ions with turning points on the low field side of the resonance, $\Lambda > \Lambda_{res}$.

In our model, we wish to describe both thermal and fast ions using (23). For this reason, we generalise the temperatures $T_{\perp}$ and $T_{\parallel}$ to be functions of the velocity. We set $T_{\perp} = -[\partial_W \ln \eta]^{-1}$, which can be interpreted as a *local* temperature, or slope, of the velocity distribution function. The pitch angle dependence in the distribution function has different behaviour above and below the critical velocity, $V_{\gamma}$, given by [29]. Below the critical velocity, rapid pitch angle scattering ensures an isotropic distribution function, whereas above the critical velocity, the parallel temperature is mostly unaffected by the pitch angle scattering [30]. We therefore propose that $T_{\parallel}(v)$ is limited by the critical energy $W_{\gamma} = mV_{\gamma}^2/8$ [29]. An example of the modified Dendy distribution, $\chi$, can be found in figure 2. Note that at very high energies, the peak-width in $\Lambda$ is limited to a small but finite value in order to resolve the distribution function numerically.

## 3. The Foppler code

With this paper we introduce a new code called Foppler. The code is implemented in MATLAB, is object oriented, and computes the quasi-linear diffusion coefficients and solutions in parallel on CPUs. It solves the bounce averaged and pitch angle averaged *Fokker–Planck* equation (22) for each flux surface and each ion species while including *Doppler* physics, hence the name. In this work, the quasi-linear operator is calculated using electric wave fields computed by the FEMIC code [22]. FEMIC is a full-wave solver that uses COMSOL

Multiphysics to compute the electric wave fields in two-dimensional axisymmetry, assuming Maxwellian distribution functions of all plasma populations. However, FEMIC does not account for the modification of the dielectric response due to the non-Maxwellian distributions calculated with Foppler. Consequently, the wave absorption in Foppler, is not fully consistent with the absorption in FEMIC. To address this inconsistency, the quasi-linear coefficients are normalised by a factor $C_P$ on each flux surface, i.e. $D(v, \psi) \rightarrow C_P(\psi)D(v, \psi)$ and $d(v, \psi) \rightarrow C_P(\psi)d(v, \psi)$. The value of $C_P$ is selected such that the flux surface averaged absorbed power from Foppler matches the corresponding value from FEMIC. Further details of this procedure are provided in appendix B.

### 3.1. Modelling without Doppler effects

In order to assess the importance of the Doppler shift during ICRH, simulations with the RF diffusion and drift coefficients (20) and (21) are compared with simulations with the coefficients proposed by Stix [29], which are also the basis for both the PION [13] and the FoPla [14] codes. Excluding Doppler effects, the quasi-linear diffusion coefficient is given by

$$D \propto \left| \frac{ZeE_e}{m} \right|^2 \qquad (24)$$

and the drift $d = 0$. In this model, Doppler effects are not included, thus particles resonate with the wave at the cold resonance, $\omega = n\Omega_c$. However, on flux surfaces where no such resonance can be found, the diffusion coefficient is evaluated at the point on the flux surface that is the closest to the resonance. Both diffusion coefficients, with and without Doppler effects, are normalised to absorb the same RF power density.
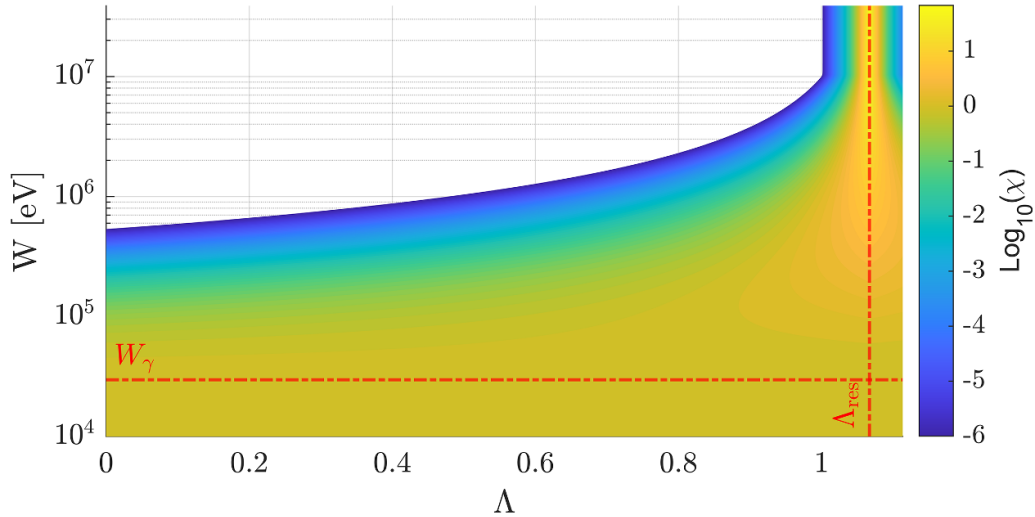
**Figure 2.** Example of the modified Dendy distribution $\chi$ in $\log_{10}$ plot as function of energy $W$ and normalized magnetic moment $\Lambda$. The value of $\Lambda$ for trapped orbits with turning points at the cold cyclotron resonance, $\Lambda_{\text{res}}$, and the critical energy, $W_\gamma$, are indicated for reference.

Consequently, the difference between the models lies in the distribution of the absorbed power over the velocity axis.

### 3.2. Quasilinear diffusion with small Doppler effects

The pitch angle-averaged diffusion coefficient in (20) extends the model without Doppler shifts, first derived by Stix [29], by including phase integrals in toroidal geometry, Doppler shifted resonances, poloidal variations of the wave electric field, and anisotropic distributions. The model without Doppler effects can be derived from (20) under two conditions. First, variations in the wave electric field must be small over the Doppler broadened resonance. Second, the denominator in (5), $\ddot{\nu}\tau_B$, should be independent of the velocity. Assuming $B \sim 1/R$ and neglecting guiding centre drifts we obtain

$$\ddot{\nu} = \frac{n\Omega_c}{R}\frac{B_R}{B}v\xi. \tag{25}$$

In the absence of Doppler shifts the explicit velocity dependence in $\ddot{\nu}$ cancels out the velocity dependence in $\tau_b$.

However, when Doppler shifted resonances are considered, an implicit velocity dependence arises in the expression for $\ddot{\nu}$. This is because all quantities must be evaluated at the Doppler shifted resonance positions, which are themselves velocity dependent, i.e. $\theta_{\text{res}}(v)$. The most significant velocity dependence is found in the ratio $B_R/B$ in (25), which projects the parallel velocity onto the major radius direction. This ratio changes on the scale lengths of the minor radius, $r$. Consequently, the diffusion coefficient without Doppler shifts can only be recovered for Doppler shifts smaller than $r$. A more detailed analysis of the variations in $B_R/B$ suggests that $\ddot{\nu}\tau_B$ is constant when

$$v \ll \frac{\omega}{k_\parallel}\frac{r}{R}. \tag{26}$$

The diffusion coefficient without Doppler effects can be derived from (20) by expanding $B(\theta_{\text{res}})$ around the cold resonance. Including linear terms in the expansion and assuming a constant $E_e$ gives a velocity independent diffusion coefficient,

$$D = \sum_n \frac{4}{3}\left|\frac{ZeE_e}{m}\right|^2\left|\frac{1}{\omega}\frac{L}{\ell}\frac{B_0}{B_\theta}\frac{B_0}{dB/d\theta}\right|. \tag{27}$$

This diffusion coefficient recovers the functional dependence proposed by Stix, while still including phase integrals in toroidal geometry.

However, when including higher-order terms in the expansion of $B(\theta_{\text{res}})$ gives an additional velocity dependence that is not present in (24). These terms represent the bending of the flux surfaces, which impacts the quasilinear diffusion through $B_R(\theta_{\text{res}}(v))/B$ in (25).

## 4. Effects of Doppler shifts on quasi-linear diffusion

In this section, the effects on the diffusion coefficient described in section 3.2 are illustrated for a JET deuterium plasma with a 3 % hydrogen minority. The electron density is $5 \times 10^{19}\,\text{m}^{-3}$, the ion and electron temperatures are 4 keV, the waves have a frequency of 50 MHz, and the toroidal mode number is $n_\phi = 27$.

Figure 3 shows the quasilinear diffusion coefficient when the cold resonance is centred on the magnetic axis. For illustration, we have selected the flux surface $\rho = 0.2$, where the cold resonances are found above and below the magnetic axis. Note that on other flux surfaces or in other scenarios, the diffusion coefficient may differ quantitatively. Here, finite Larmor radius (FLR) effects are disabled for clarity. This corresponds to setting $k_\perp = 0$, or the effective electric field strength $E_e = E_+$. The figure shows four diffusion coefficients calculated under different assumptions. The blue
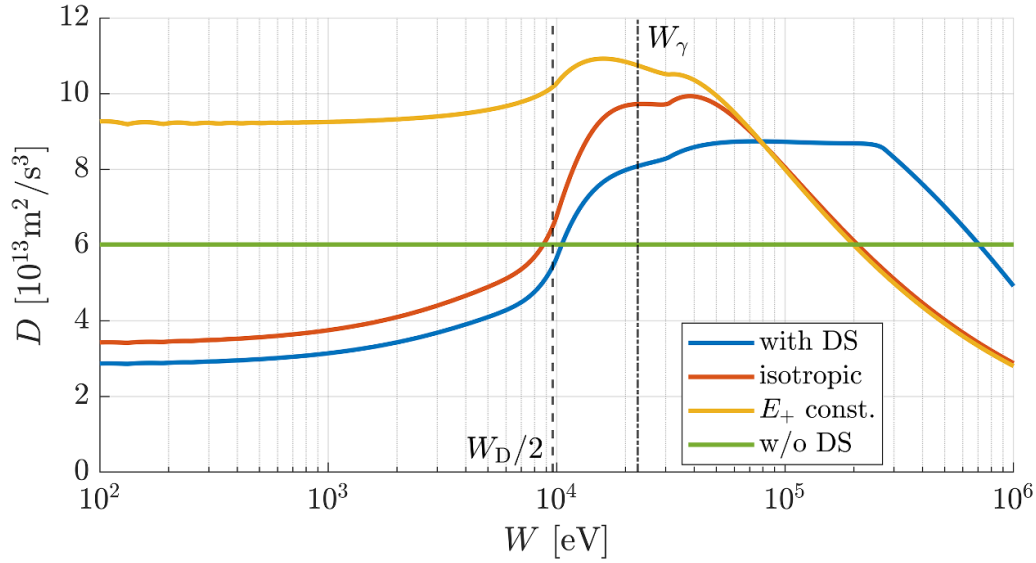
**Figure 3.** Example for the effects on the quasi-linear diffusion coefficient for a minority heating scenario in a JET-like plasma for $n_\phi = 27$ on the flux surface $\rho = 0.2$. Here, FLR effects are neglected for clarity. The blue curve shows the coefficient (20) with Doppler shifts (DS), phase integrals in toroidal geometry, poloidal variations of the wave electric field, and the anisotropic pitch angle distribution. The red curve shows the coefficient but with an isotropic pitch angle distribution. The yellow curve illustrates the case of isotropic pitch angle distributions for constant electric fields, but with phase integrals in toroidal geometry. The coefficient without Doppler shifts is shown in green.

curve shows the full diffusion coefficient given by (20), for a power density of $0.44\ \mathrm{MW\,m^{-3}}$, including the Dendy model for the anisotropy. When the Dendy model is replaced by an isotropic distribution we move from the blue to the red curve. Here we tend to overestimate the effects of the Doppler shift above the critical energy $W_\gamma$. There are two reasons. First, the isotropic model overestimates the number of ions with large $v_\parallel$ and large Doppler shifts, such that the resonance condition is no longer fulfilled on the flux surfaces. Second, the anisotropy accumulates particles around trapped orbits with turning points near the cold resonance, where the wave-particle interaction is strong. Note that the power normalization $C_{\mathrm{P}}(\psi)$ rescales the diffusion coefficients to absorb the same power density, i.e. boosting the diffusion in the red curve to compensate for the lower diffusion above $W_\gamma$.

The yellow curve is again calculated for an isotropic distribution, but here the electric field, $E_+$ has artificially set to a constant value. Comparing this yellow curve with the red curve we conclude that the poloidal variations in $E_+(\theta_{\mathrm{res}})$ can significantly alter the quasilinear diffusion. In fact, while ions around 1 keV absorb near the cold resonance, ions around 20 keV absorb mainly near the ion-ion hybrid layer where the polarisation is more favourable. As a reference, the diffusion coefficient without Doppler effects, (24), is shown in green.

Figure 3 also indicates the energy $W_{\mathrm{D}}/2 \approx 6$ keV (where $W_{\mathrm{D}} = 1/2\,m(\omega/k_\parallel)^2(r/R)^2$), below which we expect the model without Doppler shifts to be valid at constant $E_+$. Indeed, below this energy the model without Doppler shifts (green curve) agrees with the yellow curve that includes Doppler shifts, except that different normalisations, $C_P$, have been applied.

## 5. Application to the three-ion scenario

In this section, we apply the Foppler code to study three-ion heating [31] in a JET-like plasma. This is a scenario where Doppler effects are particularly important. The RF waves have a frequency of 32.5 MHz with a toroidal mode number $n_\phi = 27$. The plasma is composed of 71% hydrogen, 29% deuterium and small traces of $^3$He, which should maximize the $^3$He absorption [31]. We use parabolic density and temperature profiles, where the on-axis electron density is $4 \times 10^{19}\ \mathrm{m^{-3}}$ and the on-axis ion and electron temperatures are 4 keV.

In the remainder of this chapter, we study how the Doppler shifts influence the collisionally transferred power, distribution functions and the quasi-linear RF diffusion coefficients. This permits the DEMO of the abilities of the Foppler code, and the importance of the Doppler shifts.

### 5.1. Collisional power transfer

One of the main goals of ICRH is heating of the thermal ion species to high temperatures. Our model describes how wave power is absorbed by ions and how the power is transferred to the thermal plasma through collisions. Here we are particularly interested in the fraction of the heating power that is collisionally transferred to each plasma species.

In the three-ion scenario, the concentrations of the majority species (here H,D) are selected such that the L-cutoff falls on the cold resonance position of a third ion species (here $^3$He). Consequently, the polarization of the wave field is favourable at the resonance of the third ion species. This effect is illustrated in figure 4, showing the left-hand polarised electric field component, $E_+$. In figure 4(a) the $^3$He concentration is 0.005%, yielding a maximum in $E_+$ at the cold cyclotron
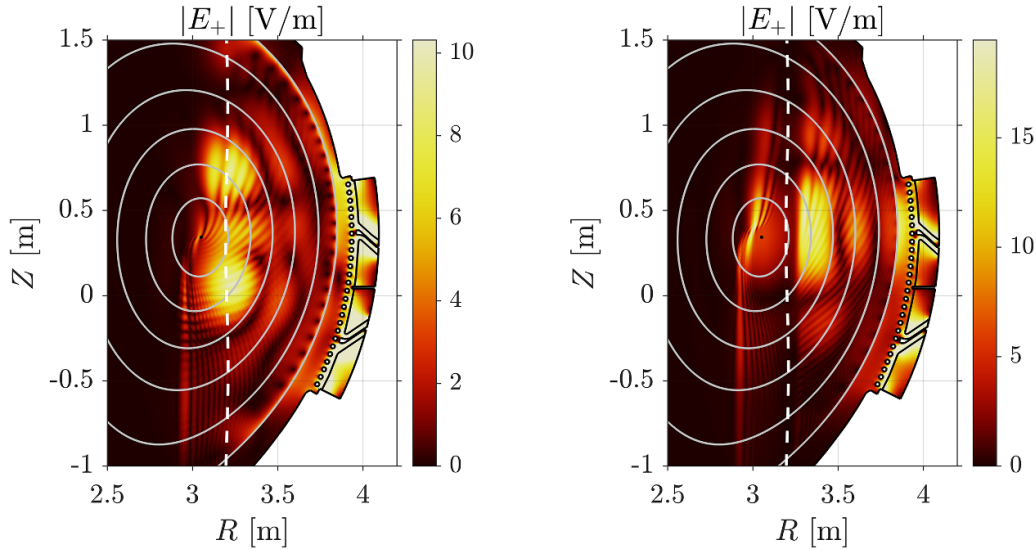
**Figure 4.** Absolute value of the left-hand circularly polarised component of the electric wave field as calculated with FEMIC for the three-ion scheme for $^3$He concentration of 0.005% on the left (a) and 0.5% on the right (b). The cold resonance position of $^3$He is marked with a white dashed line in each sub figure.

resonance. However, when increasing the concentration to 0.5% $^3$He, the polarisation is modified to reduce $E_+$ at the cold resonance, as shown in figure 4(b). At this concentration, two IIHLs appear on the high and low field side of the cold $^3$He resonance, causing strong spatial variations in $E_+$.

Increasing the concentration further, to around 1.7% $^3$He and higher, results in a transition from the three-ion scheme to a so-called inverted scenario [32]. In this case, the wave encounters an evanescent layer before it reaches the cold resonance position of $^3$He. The resulting wave reflection decreases power absorption in the plasma significantly, making such scenarios inefficient for plasma heating.

In the case of 0.5% $^3$He, the value of $|E_+|^2$ is two orders of magnitude smaller at the cold resonance compared to the value at the nearby maximum. Thus, Doppler-shifted resonances with an anisotropic pitch angle distribution are particularly important for the diffusion coefficient. This effect is illustrated in figure 5, where the $^3$He concentration and the coupled power are simultaneously changed to keep the power per particle constant.

We observe that for $^3$He concentrations below 0.4%, the model with and without Doppler effects agree. However, above 0.4% the models start to diverge and at 1% the model with Doppler effects predicts four times more electron heating than the model without Doppler effects. At 1 MW total absorbed wave power and 0.5% $^3$He, 96% of the wave power is absorbed by $^3$He as seen from the black curve. Out of this power, Foppler predicts that 42% is transferred to the electrons, compared to 34% when Doppler shifts are neglected.

In figure 6, it can be seen that for 0.5% $^3$He (1 MW), this difference is localised to two regions in the plasma. The collisional power transfer to electrons (shown in yellow) is increased and the transfer to ions (shown in red and blue) is decreased due to Doppler shifts, both in the centre, $\rho \in [0, 0.15]$, and farther out, $\rho \in [0.32, 0.45]$, where $\rho$ is the poloidal flux coordinate. Note that with consistent coupling of

FEMIC and Foppler the fraction of power absorbed by $^3$He will likely change, see the black curves in figures 5 and 6. In particular, this change may differ between the models with and without Doppler-shift. This is going to be investigated in future work.

## 5.2. Distribution functions and quasi-linear diffusion coefficients

The observed differences between modelling with and without Doppler shift are particularly prominent on the flux surfaces where $\rho = 0.05$ and $\rho = 0.39$, as shown in figure 6. The following analysis therefore focuses on these two flux surfaces.

In figure 7, the distribution functions calculated with Doppler shifts are increased at energies above circa 50 keV compared to the ones calculated without Doppler shifts. This corresponds to an increased number of fast ions and a decreased number of thermal ions.

The reason for this can be investigated by studying the quasi-linear diffusion coefficient from equation (20) shown in figure 8. The discussion in section 4 on figure 3 is also applicable here. Additionally, FLR effects appear in the Bessel functions of $E_e$ for both models with and without Doppler effects. This can be seen in the dashed curves in figure 8 above 1 MeV. The diffusion coefficients with Doppler shifts (solid curves in figure 8) exhibit an increase over the range from 2–20 keV. At $\rho = 0.39$ this increase is mainly due to Doppler shifted interactions at a more favourable polarisation, i.e. a stronger $E_+$. At $\rho = 0.1$ the reason is quite different. Here the cold resonance does not intersect the flux surface, thus only ions above 3 keV can have sufficient Doppler shift to resonate with the wave. In the 10 keV and 100 keV range, the anisotropic pitch distribution boosts the diffusion coefficient, as described in section 4. Above 500 keV, the diffusion coefficient at $\rho = 0.39$ with Doppler shift starts to decrease. This is associated to the
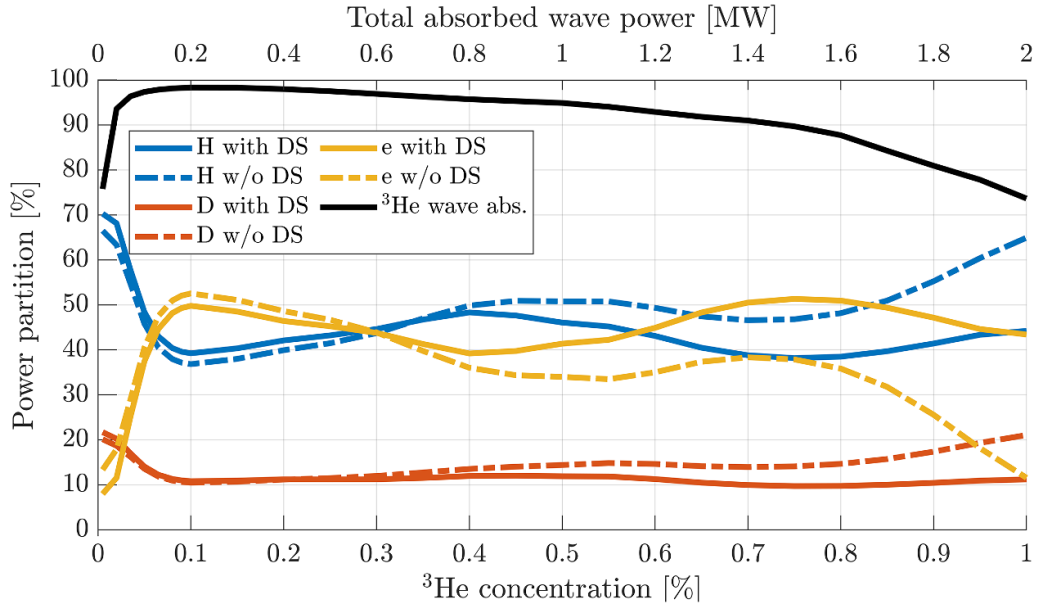
**Figure 5.** Collisional power transfer to hydrogen (H), deuterium (D) and electrons (e) with and without Doppler shift (DS). The ratio of total absorbed power to $^3$He concentration is kept constant, which is expressed with the two horizontal axes. The black curve shows the fraction of the wave power absorbed by $^3$He.
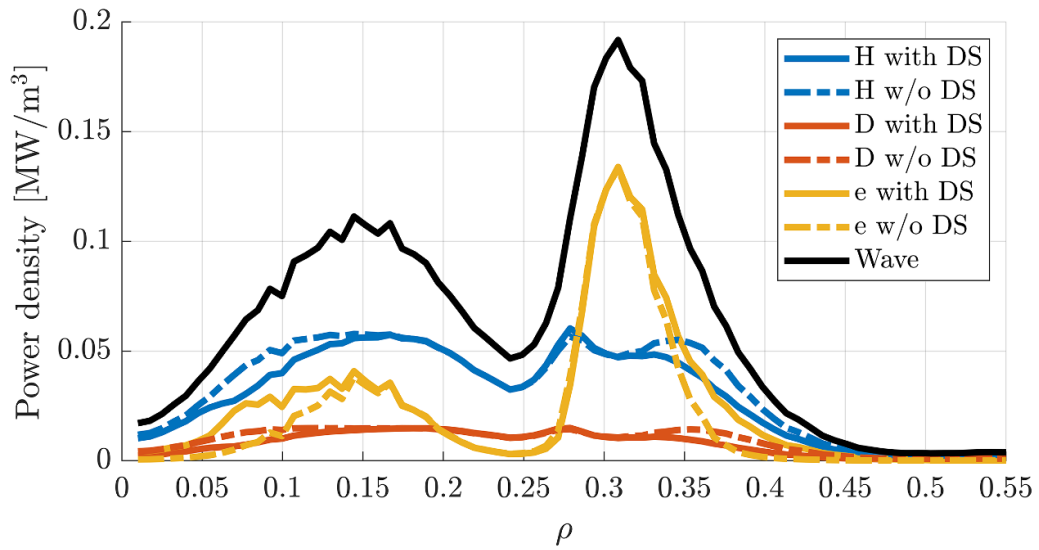


**Figure 6.** Collisional power transfer profiles in the three-ion scenario at 1 MW and 0.5% $^3$He concentration, plotted for different plasma species with and without Doppler shift (DS). The flux surface averaged power deposition from the wave to $^3$He is plotted in black.

further narrowing down of the pitch angle distribution around $\Lambda = \Lambda_{\mathrm{res}}$. These fast ions do not have sufficiently large parallel velocities to resonate in the regions with strong $E_+$.

We can conclude that diffusion can be enhanced or reduced in certain energy regimes due to Doppler effects. However, there cannot be an overall increased or decreased diffusion, because the quasi-linear coefficients are normalised for each model to match the absorbed wave power by FEMIC. The normalisation moderates the impact of the omission of Doppler effects on velocity space integrated quantities, such as the collisional power transfer to ions and electrons. Nonetheless, Doppler effects may have a significant impact on the velocity distribution locally in velocity.

The enhanced diffusion regime due to Doppler effects is situated largely above the critical energy of circa 30 keV as seen in figure 8. This causes an increased fast ion population above the critical energy due to Doppler effects as shown in figure 7. For energies above the critical energy, fast ions slow down predominantly on electrons, which increases the electron heating as seen in figure 6.

In summary, it is observed that in these cases, Doppler shifts enhance power absorption at energies above the critical energy. In turn, this results in larger fast ion populations. Consequently, collisional power transport to electrons is increased on certain flux surfaces. This increases the overall volume integrated power transmitted to electrons, too, which
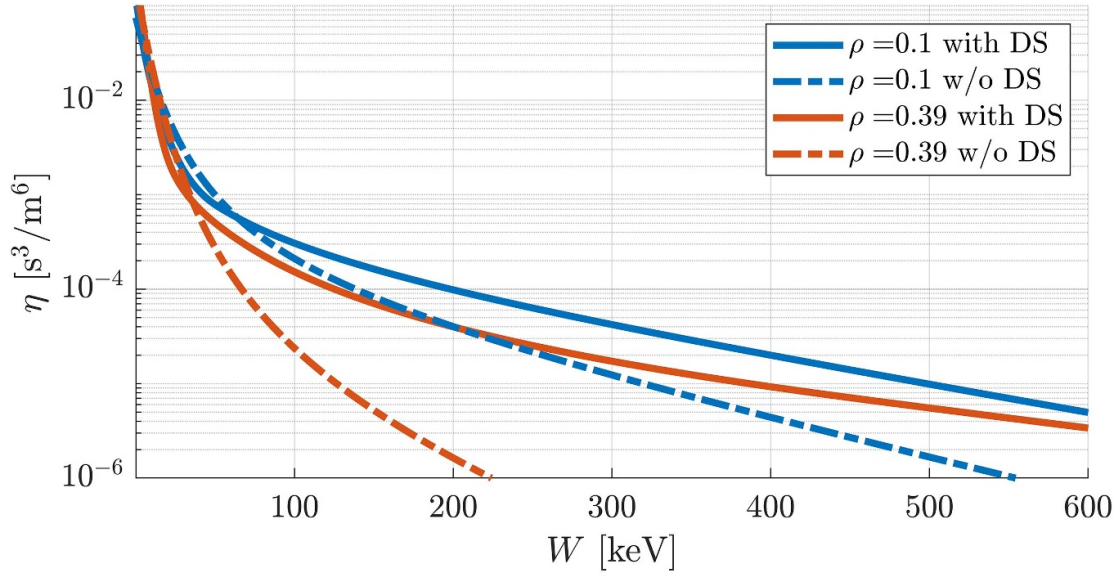
**Figure 7.** Distribution functions of $^3$He in the three-ion scenario at 1 MW and 0.5% $^3$He concentration on two different flux surfaces $\rho$ with and without Doppler shift (DS).



**Figure 8.** Quasi-linear diffusion coefficients of $^3$He in the three-ion scenario at 1 MW and 0.5% $^3$He concentration on two different flux surfaces $\rho$ with and without Doppler shift (DS). The critical energies $W_\gamma$ on both flux surfaces are in the shaded grey area.
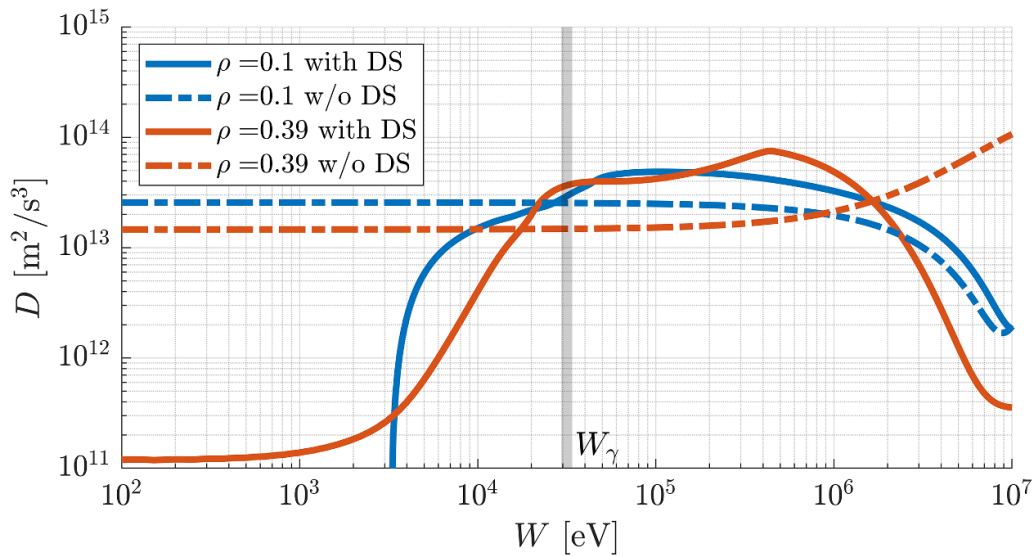
alters the power partition. These Doppler effects can become significant as shown in figure 5. Such effects are non-linear and sensitive to wave polarization patterns, total absorbed power and minority concentrations, among others. The normalisation procedure to match the flux surface averaged power absorption of the Fokker–Planck model with the wave solver moderates the differences between different Fokker–Planck models.

## 6. Discussion and conclusion

In this report a new formulation of a pitch-angle averaged Fokker–Planck equation, combined with a model for the anisotropy of the pitch angle distributions, has been used to study

the impact of Doppler effects on the distribution of ICRH accelerated ions. The main conclusion from this study is that the Doppler effects can play an important role, in particular in the presence of highly inhomogeneous wave fields. Two examples are studied in this work, the three-ion scheme and minority scheme with a prominent ion-ion hybrid layer. Under such conditions, it is shown that the quasi-linear diffusion coefficients is notably altered when Doppler shifts are included. This modification, in turn, affects the velocity distribution function, leading to changes in the collisional power density transferred from the resonating species to background ions and electrons.

For this study, a new model has been developed to include Doppler effects. The key technical step in deriving the pitch

angle averaged distribution function with anisotropic pitch angle distributions involved transforming an integral over the generalised pitch angle variable, $\Lambda$, to an integral over the poloidal angle at the resonance of the ions. This made it possible to resolve apparent singularities of the resonant interaction time that appear at tangential resonances, where $\ddot{\nu} = 0$. The presented model for the pitch angle averaged distribution functions has been implemented in the new code Foppler.

The Doppler effects included in this model have been illustrated by comparing with a model that does not include Doppler effects; similar to the models implemented in codes such as PION [13] and FoPla [14]. We show that Doppler effects modifiy the quasilinear diffusion through both the resonant interaction time and by spatially displacing the absorption towards regions with either strong wave intensity, or more favourable polarisation. Furthermore, we show that when including Doppler effects it is important to also include the anisotropy of the distribution.

In the future, we plan to benchmark Foppler with other Fokker–Planck codes and experimental results, in order to validate the model presented in this paper. In particularly, we intend to assess the validity and possible alternatives for the pitch angle distribution.

## Data availability statement

## Acknowledgments

## Appendix A. Change of coordinate $\Lambda \to \theta_{\mathrm{res}}$

In this appendix, the derivation of the change of coordinates from the normalized magnetic moment $\Lambda$ to the resonant poloidal angle $\theta_{\mathrm{res}}$ is presented. We start by expressing a general differential of the resonance function as

$$\mathrm{d}f_{\mathrm{res}}(v, \Lambda, \psi, \theta) = \mathrm{d}(n\Omega_{\mathrm{c}}) + \mathrm{d}(k_{\parallel}v_{\parallel}) - \mathrm{d}\omega. \tag{A.1}$$

where the antenna frequency $\omega$ is constant, such that $\mathrm{d}\omega = 0$. We consider thin orbits, where $P_{\phi} = Ze\psi$ and the total velocity

$v$ are constant, while we allow changes in the resonance function due to changes in the normalized magnetic moment, $\Lambda$, and the poloidal angle $\theta$. In particular, the harmonic cyclotron frequency $\Omega_{\mathrm{c}}$ and the parallel component of the wave vector experienced by the ion, $k_{\parallel}$, as well as the parallel velocity of the ion

$$v_{\parallel}(\Lambda, \theta) = \sigma v \sqrt{1 - \frac{\Lambda B(\theta)}{B_0}} \tag{A.2}$$

may change due to variations in the magnetic moment or due to motion along the orbit. We can therefore express the change in the resonance function as

$$\mathrm{d}f_{\mathrm{res}} = \left[ \frac{nZe}{m} \frac{\mathrm{d}B}{\mathrm{d}\theta} + k_{\parallel} \frac{\mathrm{d}v_{\parallel}}{\mathrm{d}\theta} + v_{\parallel} \frac{\mathrm{d}k_{\parallel}}{\mathrm{d}\theta} \right] \mathrm{d}\theta + \left[ k_{\parallel} \frac{\mathrm{d}v_{\parallel}}{\mathrm{d}\Lambda} \right] \mathrm{d}\Lambda \tag{A.3}$$

$$\equiv f_{\theta} \mathrm{d}\theta + f_{\Lambda} \mathrm{d}\Lambda. \tag{A.4}$$

In the case of an ion moving on its unperturbed orbit for constant $(v, \Lambda, P_{\phi})$, and assuming that the change in $f_{\mathrm{res}}$ takes place over a short time $\mathrm{d}t$, equation (A.4) can be written as

$$\frac{\mathrm{d}f_{\mathrm{res}}}{\mathrm{d}t} = \ddot{\nu} = f_{\theta}\dot{\theta}. \tag{A.5}$$

The rate of change of the poloidal angle in time can be expressed as

$$\dot{\theta} = v_{\parallel} \frac{B_{\theta}}{B} \frac{2\pi}{L}, \tag{A.6}$$

where the angle $\theta$ is defined by equal arc lengths and $L$ is the total length of the flux surface in a poloidal plane. Then, we can write

$$\mathrm{d}f_{\mathrm{res}} = \frac{LB\ddot{\nu}}{2\pi v_{\parallel}B_{\theta}} \mathrm{d}\theta + f_{\Lambda} \mathrm{d}\Lambda. \tag{A.7}$$

where

$$f_{\Lambda} = k_{\parallel} \frac{\mathrm{d}v_{\parallel}}{\mathrm{d}\Lambda} = -\frac{v^2 k_{\parallel} B}{2 v_{\parallel} B_0}. \tag{A.8}$$

Now we restrict the differentials to obtain the relation between $\Lambda$ and $\theta_{\mathrm{res}}$. We consider only values of $\theta$ and $\Lambda$ where $f_{\mathrm{res}} = 0$, the ion is in resonance and therefore $\theta = \theta_{\mathrm{res}}$. Assuming that the resonance condition remains fulfilled, then $\mathrm{d}f_{\mathrm{res}} = 0$ and it can be observed how a change in $\theta_{\mathrm{res}}$ relates to a change in $\Lambda$. This corresponds to observing how the resonance moves along the flux surface when the normalised magnetic moment, i.e. the ion orbit, is changed. Now the relation that describes the change of coordinates from $\Lambda$ to $\theta_{\mathrm{res}}$ is obtained,

$$\mathrm{d}\Lambda = \frac{LB_0\ddot{\nu}}{\pi v^2 k_{\parallel}B_{\theta}} \mathrm{d}\theta_{\mathrm{res}}. \tag{A.9}$$

## Appendix B. Power normalisation procedure

To ensure consistency between the wave code FEMIC and the Fokker–Planck code Foppler with respect to the flux surface averaged power absorption of each species, a power normalisation procedure is applied. This procedure aligns the power absorption calculated by Foppler with that predicted by FEMIC. The flux surface averaged power absorption in Foppler, $P_{Q,\text{FP}}$, is computed as the energy moment of the quasi-linear operator

$$P_{Q,\text{FP}}(\psi) = \int_0^\infty \frac{mv^2}{2} \langle\langle Q(f_0)\rangle\rangle_\Lambda 4\pi v^2 \mathrm{d}v, \qquad \text{(B.1)}$$

where $\langle\langle Q(f_0)\rangle\rangle_\Lambda$ represents the quasi-linear operator from equation (13), which depends on the velocity $v$ and is evaluated for each ion species on each flux surface $\psi$. This power density is then matched to the corresponding value predicted by FEMIC, $P_{Q,\text{WS}}$, using a normalisation factor

$$C_\text{P}(\psi) = \frac{P_{Q,\text{WS}}}{P_{Q,\text{FP}}}. \qquad \text{(B.2)}$$

The quasi-linear coefficients $D$ from equation (14) and $d$ from equation (15) are subsequently normalised by this factor for each flux surface and species. The resulting quasi-linear operator is therefore implicitly defined by

$$\langle\langle Q(f_0)\rangle\rangle_\Lambda = \left[ \frac{P_{Q,\text{WS}}}{\int \langle\langle Q(f_0)\rangle\rangle_\Lambda 2\pi m v^4 \mathrm{d}v} \right]$$
$$\times \frac{1}{v^2} \frac{\partial}{\partial v} v^2 \left( \mathrm{d}\eta + D \frac{\partial\eta}{\partial v} \right). \qquad \text{(B.3)}$$

To solve the Fokker–Planck equation with this normalised quasi-linear operator, an iteration scheme is employed. Initially, the distribution is assumed to be Maxwellian to calculate the absorbed power from equation (B.1). The quasi-linear operator is then normalised as described in equation (B.3) and the velocity distribution is recalculated. These steps are repeated iteratively until the normalisation factor $C_\text{P}(\psi)$ (B.2) converges. This ensures that the flux surface averaged power density is consistent between the wave solver FEMIC and the Fokker–Planck model Foppler.

## ORCID iDs

Lukas Bähner ⓘ https://orcid.org/0009-0005-5616-0235
Thomas Johnson ⓘ https://orcid.org/0000-0002-7142-7103
Lars-Göran Eriksson ⓘ https://orcid.org/0009-0004-1375-9929
Björn Zaar ⓘ https://orcid.org/0000-0002-3280-2361

## References

[1] Start D *et al* 1998 *Phys. Rev. Lett.* **80** 4681
[2] Start D *et al* 1999 *Nucl. Fusion* **39** 321
[3] Wilson J *et al* 1995 *Phys. Rev. Lett.* **75** 842
[4] Gormezano C *et al* 2007 *Nucl. Fusion* **47** S285
[5] Wilson J and Bonoli P 2015 *Phys. Plasmas* **22** 021801
[6] Jacquinot J *et al* 1999 *Nucl. Fusion* **39** 2495–539
[7] Lerche E *et al* 2016 *Nucl. Fusion* **56** 036022
[8] Jucker M, Graves J, Cooper W, Mellet N, Johnson T and Brunner S 2011 *Comput. Phys. Commun.* **182** 912–25
[9] Choi M *et al* 2010 *Phys. Plasmas* **17** 090701
[10] Hedin J, Hellsten T, Eriksson L G and Johnson T 2002 *Nucl. Fusion* **42** 527
[11] Schneider M *et al* 2016 *Nucl. Fusion* **56** 112022
[12] Petrov Y V and Harvey R 2016 *Plasma Phys. Control. Fusion* **58** 115001
[13] Eriksson L G, Hellsten T and Willén U 1993 *Nucl. Fusion* **33** 1037
[14] Van Eester D, Lerche E, Huynh P and Johnson T (EUROfusion-IM team) 2021 *J. Plasma Phys.* **87** 855870202
[15] Eriksson L G and Helander P 1994 *Phys. Plasmas* **1** 308–14
[16] Hellsten T, Carlsson J and Eriksson L G 1995 *Phys. Rev. Lett.* **74** 3612
[17] Eriksson L G *et al* 1998 *Phys. Rev. Lett.* **81** 1231
[18] Mantsinen M *et al* 2002 *Phys. Rev. Lett.* **89** 115004
[19] Eriksson L G *et al* 2006 *Nucl. Fusion* **46** S951
[20] Graves J *et al* 2012 *Nat. Commun.* **3** 624
[21] Dendy R, Hastie R, McClements K and Martin T 1995 *Phys. Plasmas* **2** 1623–36
[22] Vallejos P, Johnson T, Ragona R, Hellsten T and Frassinetti L 2019 *Nucl. Fusion* **59** 076022
[23] Bécoulet A, Gambier D and Samain A 1991 *Phys. Fluids B: Plasma Phys.* **3** 137–50
[24] Helander P and Lisak M 1992 *Phys. Fluids B: Plasma Phys.* **4** 1927–34
[25] Bergeaud V, Nguyen F, Bécoulet A and Eriksson L G 2001 *Phys. Plasmas* **8** 139–45
[26] Bernstein I B and Baxter D C 1981 *Phys. Fluids* **24** 108–26
[27] Stix T 1992 *Waves in Plasmas* (Springer & Business Media)
[28] Kasilov S, Pyatak A and Stepanov K 1990 *Nucl. Fusion* **30** 2467
[29] Stix T 1975 *Nucl. Fusion* **15** 737
[30] Kerbel G and McCoy M 1985 *Phys. Fluids* **28** 3629–53
[31] Kazakov Y, Van Eester D, Dumont R and Ongena J 2015 *Nucl. Fusion* **55** 032001
[32] Mayoral M L *et al* 2006 *Nucl. Fusion* **46** S550